García-Pardo, JG.; Colomer, A.; Naranjo Ornedo, V.; Peñaranda, F.; Sales, MÁ. (2018). Identification of Individual Glandular Regions Using LCWT and Machine Learning Techniques. En Intelligent Data Engineering and Automated Learning – IDEAL 2018. Springer. 642-650. https://doi.org/10.1007/978-3-030-03493-1_67

Identification of individual glandular regions using LCWT and machine learning techniques

José Gabriel García[1], Adrián Colomer[1], Valery Naranjo[1], and Francisco Peñaranda[1]

[1] Instituto de Investigación e Innovación en Bioingeniería (I3B), Universitat Politècnica de València, Camino de Vera s/n, 46022, Valencia, Spain.
jogarpa7@i3b.upv.es

Abstract. A new approach for the segmentation of gland units in histological images is proposed with the aim of contributing to the improvement of the prostate cancer diagnosis. Clustering methods on several colour spaces are applied to each sample in order to generate a binary mask of the different tissue components. From the mask of lumen candidates, the Locally Constrained Watershed Transform (LCWT) is applied as a novel gland segmentation technique never before used in this type of images. 500 random gland candidates, both benign and pathological, are selected to evaluate the LCWT technique providing results of Dice coefficient of 0.85. Several shape and textural descriptors in combination with contextual features and a fractal analysis are applied, in a novel way, on different colour spaces achieving a total of 297 features to discern between artefacts and true glands. The most relevant features are then selected by an exhaustive statistical analysis in terms of independence between variables and dependence with the class. 3.200 artefacts, 3.195 benign glands and 3.000 pathological glands are obtained, from a data set of 1468 images at 10x magnification. A careful strategy of data partition is implemented to robustly address the classification problem between artefacts and glands. Both linear and non-linear approaches are considered using machine learning techniques based on Support Vector Machines (SVM) and feedforward neural networks achieving values of sensitivity, specificity and accuracy of 0.92, 0.97 and 0.95, respectively.

Keywords: Machine learning, multi-layer perceptron, support vector machine, locally constrained watershed transform, gland unit identification, histological prostate image

1 Introduction

The definitive diagnostic procedure to detect prostate cancer is the visual examination of biopsy samples stained with hematoxylin and eosin (H&E). From these digital images, pathologists assign a score according to the Gleason classification system [1], such that Gleason grades 1 and 2 correspond to benign samples, whereas grades 3, 4 and 5 correspond to malignant samples. Thereby,

histological images are essential for the physicians to make a reliable and accurate diagnosis of the patient. However, this manual task is time-consuming, tedious and subjective, which results in high rates of discordance between different pathologists.

Several studies on computer-aided Gleason grading have been developed to help the pathologists and to reduce the subjectivity level. The standard procedure starts by segmenting some individual glands, and then, these segmented glands are classified into their corresponding grades through a feature extraction step [2], [3], [4]. However, a recent study [5] claimed that to achieve significant improvements in the Gleason score discrimination, it is essential to perform an initial accurate segmentation of individual glandular regions like the one shown in Fig. 1. Motivated by such statement, this paper focuses on the identification and segmentation of each gland unit.

The proposed model to segment glands previously requires the accurate detection of lumens, which can be often confused with an artefact by its white colour. Nevertheless, an artefact is not surrounded by cytoplasm and nuclei components [3], as can be observed in Fig. 1. In this study, all lumen candidates are segmented, and then, a classification stage is carried out by means of different machine learning techniques widely used in the literature [4], in order to discern between artefacts and true glands.

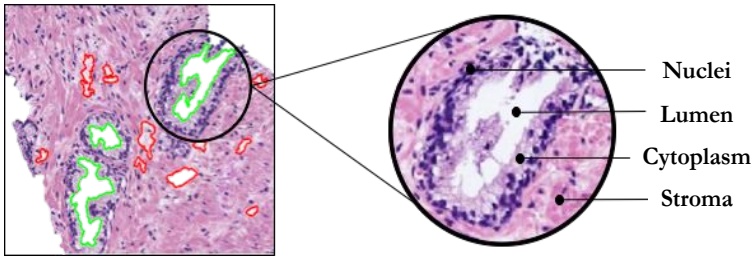

Fig. 1. The left image shows examples of lumens (green) and artefacts (red). The right image corresponds to an individual glandular region.

2 Methodology

2.1 Material

The data set used in this paper includes 854 benign and 614 grade 3 pathological images, according to the Gleason scale, at 10x magnification with an image size of $1024 \times 1024 \times 3$ pixels, providing a total of 3.200 artefacts, 3.195 benign glands and 3.000 pathological glands. The samples come from a private database of the *Hospital Clinico Universitario de Valencia*, and they are characterised by a high variability both in shape and size of glands, as well as colour and sharpness of tissues, in order to provide a robust and consistent model.

2.2 Clustering

A clustering algorithm based on the *k-means* technique is carried out on several colour spaces. In particular, it is performed in Red, Green and Blue components from RGB colour spaces, Cyan from CMYK and Saturation from HSV, with the aim of grouping the pixels into four clusters: lumen, stroma, cytoplasm and nuclei, as shown in Fig. 2. In this way, each pixel is assigned to the cluster label with the closest centroid.

Notably, the resulting image of lumen candidates provides a large quantity of artefacts (see Fig. 2). For this reason, a filtering operation based on mathematical morphology, *area opening* [6], is used to remove the connected components whose number of pixels is smaller than a specific threshold $s = 40$ pixels.

The obtained masks are used as inputs in the following segmentation and feature extraction steps to discriminate between artefacts and glands.

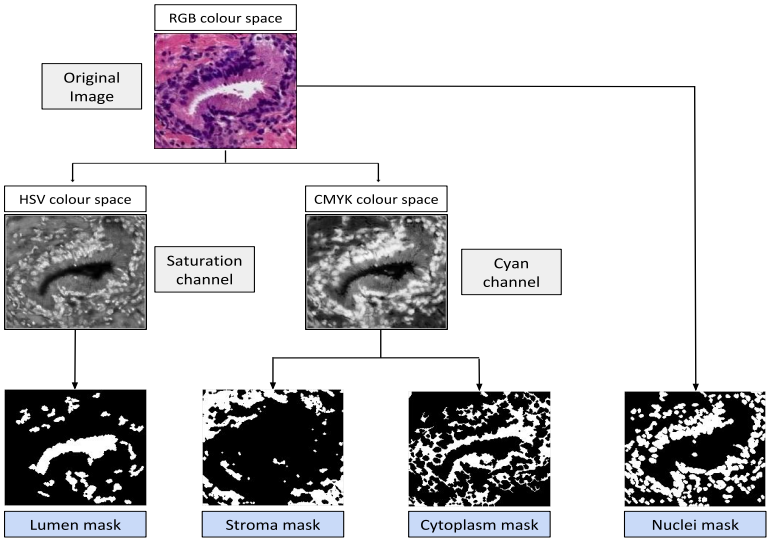

Fig. 2. Clustering procedure to obtain the different component masks by applying a transformation from RGB to CMYK and HSV colour spaces.

2.3 Gland candidates segmentation

Unlike the work presented in [2], where the gland boundaries are defined by the limits of the cytoplasm structures, in this paper a gland unit is described by its epithelial nuclei layer, similarly to the studies presented in [3] and [7] and according to the medical literature exposed in them. The three aforementioned segmentation approaches are shown in Fig. 3 to compare them.

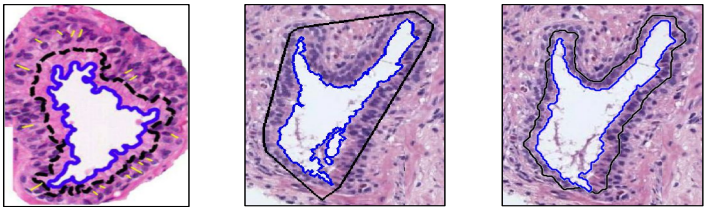

(a) (b) (c)

Fig. 3. Comparison of segmentation approaches proposed by different authors, where the blue line delimits the lumen; and the black line, the gland. (a) Example of segmented gland published in [2]. (b) Segmented gland with the code that the author proposes in [3]. (c) Same segmented gland with the method proposed in this study.

The most remarkable novelty of this paper lies in the development of a robust segmentation method, based on the Locally Constrained Watershed Transform (LCWT), able to address the delimitation of prostate glands in spite of its frontier (nuclei) remain open. [8]. LCWT requires as inputs parameters: 1) internal markers, defined by the lumen candidates mask; 2) external markers, described by the pixels associated to the stroma mask; 3) input image, defined by the nuclei mask; and 4) Structurant Elements (SE) for both markers, which specifies the step size. The algorithm is based on the fact that each marker analyses the pixels of its neighbourhood trying to incorporate them into its region. The progress in the search for the integration of new pixels is carried out such that the higher the SE is, the more pixels are incorporated. On the other hand, the nuclei (input image) act as a restriction to the markers progress. Specifically, the expansion of a marker stops when the size of its SE is greater than the distance between adjacent nuclei. In that case, the external marker can not progress and a closed line of segmentation is defined by the distance between adjacent nuclei when both markers get into contact. Thus, the segmentation is performed over the nuclei epithelial layer around the gland (See Fig. 4).

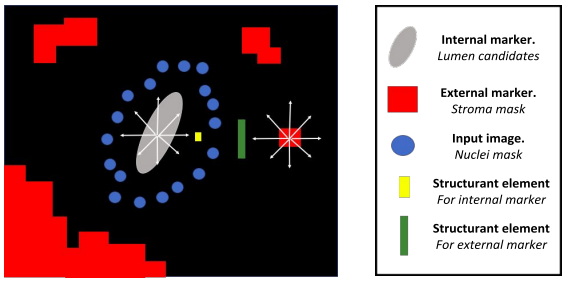

Fig. 4. Illustrative example to explain visually the performance of LCWT technique.

The detailed process is applied to the images under study of $1024 \times 1024 \times 3$ pixels to obtain the segmentation of each gland candidate. (See Fig 5).

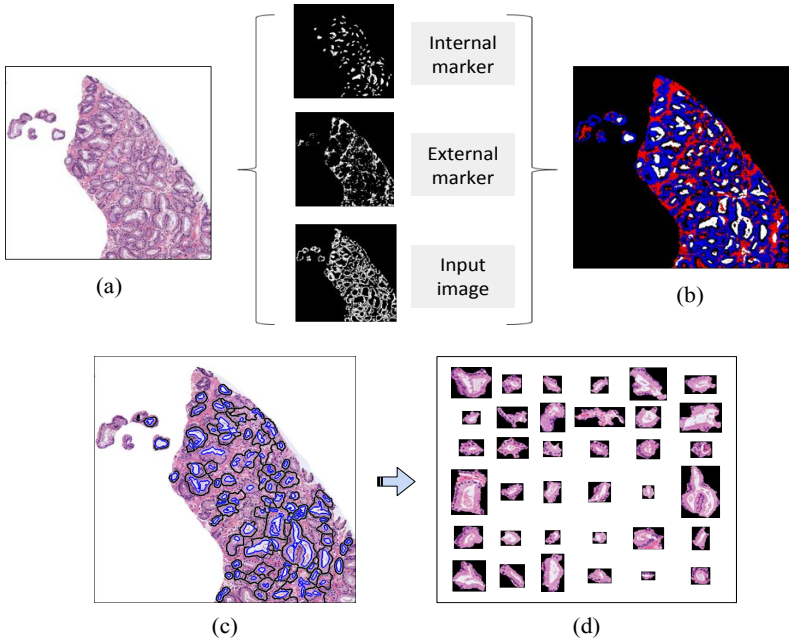

Fig. 5. (a) Original image. (b) Input parameters to the LCWT algorithm. (c) Image of $1024 \times 1024 \times 3$ pixels where all possible glands (black line) have been segmented from each lumen candidate (blue line). (d) All gland candidates automatically segmented by means the LCWT technique.

2.4 Extraction and selection of features

Once all candidates to gland are segmented, it is necessary to implement a classification stage in order to discard the artefacts. In this way, a future grading Gleason could be more efficient because the extraction and selection of features would be carried out from well-defined glands. Therefore, in this work, several descriptors are computed in order to distinguish between artefacts and glands.

On the one hand, shape descriptors are used to extract the structural and morphological information of the different components relative to the gland units and to the lumen, nuclei and cytoplasm structures. This approach was applied in some studies that also focused on the artefacts detection [7]. The metrics computed for the gland units and the lumens are: area, compactness, convex area, convex hull, eccentricity, ellipsoid diameter, extent, orientation, perimeter,

roundness and solidity. The features related to the nuclei and the cytoplasm structures make reference to the density of pixels present in the segmented region.

On the other hand, in the same way that in [9], textural descriptors related to the grey-level co-occurrence matrix (GLCM) and Local Binary Patterns (LBP) are applied in order to extract the local texture information in the images. The computed metrics from the GLCM are: contrast, correlation, energy, homogeneity, mean and standard deviation. Regarding LBP, local histograms are used as feature vectors. In particular, 10-bin $LBP^{riu2}_{P,R}$ histograms uniformly invariant to rotation transforms [10] and 10-bin $LBP^{riu2}_{P,R}$ histograms invariant against to local changes of contrast ($VAR_{P,R}$) [11].

Regarding the fractal analysis, in [12] the fractal dimension (FD) is used to analyse intensity and texture variations in certain regions of interest. In this work, the Hurst exponent is extracted over five directions (0º, 30º, 45º, 60º and 90º) with the aim of determining whether the data follow random or similar patterns. With the Hurst exponent, it is possible to analyse the complexity and the roughness character of the elements.

Finally, contextual features are also computed, similarly to [7] to consider the information around each gland candidate. In this way, relations of distances, shapes and other similarities between the individual gland and its context are taken into account.

It is important to remark that the textural descriptors and features based on fractals are applied to three colour spaces: cyan, hematoxylin and eosin. The two last channels are obtained from a method known as "colour deconvolution" that allows to separate the contributions of each staining in the H&E histopathological images [13].

From the 297 variables that compose a learning instance, an in-depth statistical analysis is performed with the aim of selecting the most relevant features. This process ensures both the discriminatory ability of the automatic models and the independence between features. First, a *Kolmogorov-Smirnov test* is used to check the normality of variables. A comparison of means using the *Student's t-test* method or a comparison of medians using the *Mann-Whitney U test* method is performed depending on whether the variable under study follows a normal distribution N(0,σ) or not. Thus, the independence of each variable concerning the class allows to determine the discriminatory capability of the variables. On the other hand, the independence between variables is assessed by calculating the correlation coefficient (R) to discard those variables with $p\text{-}value < 0.0001$ and $|R| > 0.95$. In this way, redundant information is avoided and finally, a total of 117 variables is obtained after the feature selection step.

2.5 Classification strategy

An exhaustive data partition process is carried out in order to build robust models and to provide reliable results. To the best of the author knowledge's, this work is the first that implements a type of data separation taking into account the medical history of the patient. In this study, all gland candidates

that belong to a certain medical history must be contained in the same data set. Thereby, different samples of a certain patient can only be used to train or to test the models, but never for both in the same iteration. Taking into account these conditions, an external cross-validation technique with $k = 5$ folds is used to divide the samples into a test set and a training set. Moreover, the training set is subdivided into train and validation sets using an internal cross-validation with $v = 10$ folds. Thereby, the method to separate the data guarantees that in each of the five external iterations, the models are evaluated with samples belonging to new patients never "seen" before for the models.

Once the samples are divided into their corresponding folds, the classification problem is addressed from both linear and non-linear approaches applying popular machine learning methods such as Support Vector Machines (SVMs) with linear (LSVM) and quadratic (QSVM) kernels. SVMs are non-parametric binary classifiers that build a hyperplane to divide the input space maximising the distance of the support vectors from the different classes [11]. On the other hand, an alternative parametric approach is also considered in this work by using a Feedforward Neural Network (FNN), a.k.a. multilayer perceptron (MLP), with one hidden layer and fifteen neurons.

3 Results and discussion

Regarding the segmentation problem, 500 random glands are manually segmented in order to evaluate the LCWT automatic segmentation technique by means of similarity measures, such as the *Dice* and *Jaccard* coefficients. Some qualitative results are shown in Fig. 6. The hypothesis is that the results achieved from 500 glands can be inferred for all population (6.195 glands in this case).

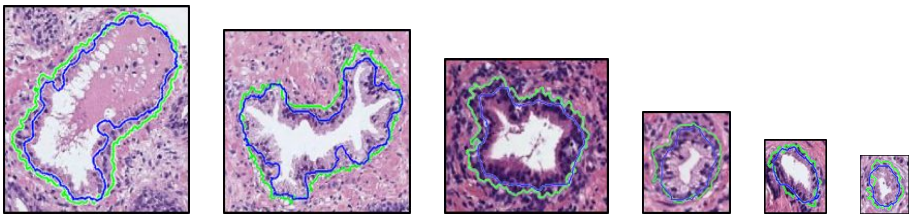

Fig. 6. Examples of benign and pathological glands of different sizes, manually and automatically segmented in green and blue, respectively.

Attending to quantitative results, the LCWT method provides a *Dice* coefficient of 0.849 and a *Jaccard* coefficient of 0.738, from 500 randomly selected glands. The *Jaccard* index is compared with the results provided by other authors in the state of the art that also consider the problem of artefacts (see Table 1). Note the data set of images used to compare is different, so the results of the segmentation can't definitively determine the best method.

Table 1. Comparison of segmentation methods with respect to the state of the art.

	Naik et al. [2]	**Nguyen et al. [7]**	**LCWT method**
***Jaccard* coefficient**	0.43	0.66	**0.74**

Results of the classification problem are provided to determine whether, from the segmented gland candidates with the LCWT method, it is possible to successfully discern between artefacts and glands, based on the features detailed in Section 2.4. Different figures of merit to evaluate the robustness of the three learned models are shown in Table 2.

Table 2. Mean and standard deviation of the classification results. (PPV: Positive Predictive Value, NPV: Negative Predictive Value; AUC: Area Under the ROC Curve).

	LSVM	**QSVM**	**MLP**
Sensitivity	0.919 ± 0.012	$\mathbf{0.932} \pm 0.013$	0.923 ± 0.019
Specificity	0.968 ± 0.027	0.956 ± 0.033	$\mathbf{0.970} \pm 0.034$
PPV	0.939 ± 0.045	0.921 ± 0.059	$\mathbf{0.941} \pm 0.042$
NPV	0.956 ± 0.013	$\mathbf{0.963} \pm 0.010$	0.959 ± 0.013
F1Score	0.929 ± 0.028	0.926 ± 0.034	$\mathbf{0.932} \pm 0.029$
Accuracy	0.951 ± 0.021	0.949 ± 0.024	$\mathbf{0.954} \pm 0.021$
AUC	0.988 ± 0.008	0.988 ± 0.009	$\mathbf{0.989} \pm 0.008$

In general, all classifiers present a similar behaviour, but MLP provides a slight outperforming over the rest. Even though it is not possible to carry out a direct comparison, MLP results are examined in contrast to other studies of the state of the art as shows Table 3.

Table 3. Comparison of classification results with respect to the state of the art.

	Naik et al. [2]	**Nguyen et al. [7]**	**MLP Classifier**
Classification accuracy	0.78 ± 0.09	0.93 ± 0.04	$\mathbf{0.95} \pm 0.02$

4 Conclusions and future work

In this paper, a new method of individual glands segmentation is proposed in order to accurately detect the relevant information about the regions of interest. Several kinds of features are extracted to identify the characteristic patterns of the true glands. Finally, a classification stage is carried out to demonstrate that, from the segmented gland candidates through the LCWT method, it is possible

to discern between artefacts and true glands. The main future research line is to address the grading Gleason by means of the characterisation of the true glands extracted from the LCWT segmentation method and after performing the proposed artefact removal.

Acknowledgements. This work has been funded by the Ministry of Economy, Industry and Competitiveness under the SICAP project (DPI2016-77869-C2-1-R). The work of Adrián Colomer has been supported by the Spanish FPI Grant BES-2014-067889. We gratefully acknowledge the support of NVIDIA Corporation with the donation of the Titan Xp GPU used for this research.

References

1. Gleason, D.F.: Histologic grading and clinical staging of prostatic carcinoma. Urologic pathology (1977)
2. Naik, S., Doyle, S., Feldman, M., Tomaszewski, J., Madabhushi, A.: Gland segmentation and computerized gleason grading of prostate histology by integrating low-, high-level and domain specific information. In: MIAAB workshop. (2007) 1–8
3. Nguyen, K., Sabata, B., Jain, A.K.: Prostate cancer grading: Gland segmentation and structural features. Pattern Recognition Letters **33**(7) (2012) 951–961
4. Kwak, J.T., Hewitt, S.M.: Multiview boosting digital pathology analysis of prostate cancer. Computer Methods and Programs in Biomedicine **142** (2017) 91–99
5. Ren, J., Sadimin, E., Foran, D.J., Qi, X.: Computer aided analysis of prostate histopathology images to support a refined gleason grading system. In: SPIE Medical Imaging, International Society for Optics and Photonics (2017) 101331V–101331V
6. Soille, P.: Morphological image analysis: principles and applications. Springer Science & Business Media (2013)
7. Nguyen, K., Sarkar, A., Jain, A.K.: Structure and context in prostatic gland segmentation and classification. In Ayache, N., Delingette, H., Golland, P., Mori, K., eds.: Medical Image Computing and Computer-Assisted Intervention – MICCAI 2012, Berlin, Heidelberg, Springer Berlin Heidelberg (2012) 115–123
8. Beare, R.: A locally constrained watershed transform. IEEE transactions on pattern analysis and machine intelligence **28**(7) (2006) 1063–1074
9. Gertych, A., Ing, N., Ma, Z., Fuchs, T., Salman, S., Mohanty, S., Bhele, S., Velásquez-Vacca, A., Amin, M.B., Knudsen, B.: Machine learning approaches to analyze histological images of tissues from radical prostatectomies. Computerized Medical Imaging and Graphics **46** (2015) 197–208
10. Ojala, T., Pietikainen, M., Maenpaa, T.: Multiresolution gray-scale and rotation invariant texture classification with local binary patterns. IEEE Transactions on pattern analysis and machine intelligence **24**(7) (2002) 971–987
11. Guo, Z., Zhang, L., Zhang, D.: A completed modeling of local binary pattern operator for texture classification. IEEE Transactions on Image Processing **19**(6) (2010) 1657–1663
12. Huang, P., Lee, C.: Automatic classification for pathological prostate images based on fractal analysis. IEEE transactions on medical imaging **28**(7) (2009) 1037–1050
13. Ruifrok, A.C., Johnston, D.A., et al.: Quantification of histochemical staining by color deconvolution. Analytical and quantitative cytology and histology **23**(4) (2001) 291–299